



## Amorphous solid helium in porous media

Jacques Bossy,<sup>1</sup> Thomas Hansen,<sup>2</sup> and Henry R. Glyde<sup>3</sup>

<sup>1</sup>*Institut Néel, CNRS–UJF, BP 166, 38042 Grenoble Cedex 9, France*

<sup>2</sup>*Institut Laue-Langevin, BP 156, 38042 Grenoble, France*

<sup>3</sup>*Department of Physics and Astronomy, University of Delaware, Newark, Delaware 19716-2570, USA*

(Received 28 December 2009; revised manuscript received 6 April 2010; published 11 May 2010)

We present neutron-scattering measurements of the static structure factor,  $S(Q)$ , of helium confined in the porous media MCM-41 of pore diameter  $47 \pm 1.5$  Å. The  $S(Q)$  shows a transition from the liquid to an amorphous solid as temperature is decreased. No Bragg peaks are observed in the solid and the  $S(Q)$  of the amorphous solid differs little from that of the liquid. On freezing, a small additional intensity in  $S(Q)$  near the main peak of the liquid  $S(Q)$  is observed. The  $S(Q)$  is compared with simulations of freezing and melting in porous media. From the measurements of freezing, an approximate phase diagram is determined. A similar amorphous  $S(Q)$  is observed in 34 Å gelsil.

DOI: [10.1103/PhysRevB.81.184507](https://doi.org/10.1103/PhysRevB.81.184507)

PACS number(s): 67.80.bd, 67.80.de, 61.05.F–

### I. INTRODUCTION

Since the initial observation of a nonclassical rotational inertia (NCRI) in torsional oscillator measurements by Kim and Chan,<sup>1,2</sup> there has been great interest in possible amorphous states of solid helium.<sup>3–6</sup> An NCRI in solid helium at temperatures below  $T_c \approx 200$  mK suggests a superfluid fraction,  $\rho_S/\rho$ , below  $T_c$ . While an NCRI is verified and its temperature dependence is quite consistently reproduced in independent measurements,<sup>7,8</sup> the magnitude of  $\rho_S/\rho$  reported varies greatly, from 0.015% to 20%. This suggests that the NCRI is not an intrinsic property of perfect-crystal solid helium. Rather it suggests that the  $\rho_S/\rho$  depends upon defects in the solid,<sup>9–11</sup> for example, vacancies, dislocations, grain boundaries, and/or amorphous regions. In addition, an increase in the transverse elastic constant<sup>12</sup> is observed below  $T_c$  and near  $T_c$  there is glassy behavior and a dissipation peak<sup>6,13,14</sup> probably involving defects.

The interpretation that amorphous regions may support superflow is supported by path-integral Monte Carlo (PIMC) calculations. The calculations predict that  $\rho_S/\rho$  and the Bose-Einstein condensate (BEC) condensate fraction,  $n_0$ , in perfect crystals are vanishingly small,<sup>15–17</sup> too small to be observed. However, similar PIMC calculations<sup>15</sup> find that amorphous solid helium contains observable values of  $\rho_S/\rho$  and  $n_0$ , e.g.,  $\rho_S/\rho \approx 5–50\%$  and  $n_0 \approx 0.5\%$ . Superflow and BEC via ground-state vacancies is definitely possible.<sup>18,19</sup> However, there is currently debate whether vacancies are stable in the ground state or not.<sup>20–22</sup>

The nature of quantum solids in porous media is also of intrinsic interest. It is specifically interesting to compare measurements of  $S(Q)$  of helium in small and larger<sup>3,23</sup> pore media and to compare measurements with simulations of freezing in confinement for both classical<sup>24,25</sup> and quantum liquids.<sup>26</sup>

In this study, we show that solid helium in small pore media of pore diameter  $d \leq 50$  Å is amorphous. The static structure factor  $S(Q)$  of the amorphous solid differs little from the liquid  $S(Q)$ . When the liquid freezes  $S(Q)$  increases slightly in intensity at  $Q$  values immediately below the peak region ( $Q \approx 2.2$  Å<sup>-1</sup>) of the liquid  $S(Q)$ , characteristic of

freezing to an amorphous solid.<sup>22,24</sup> The small increase in  $S(Q)$  may indicate some longer-range atomic ordering<sup>26</sup> on length scales of 5–10 Å. In addition, the  $S(Q)$  shows that the bound or “dead” layers on the porous media walls are amorphous. Direct comparison with simulated values<sup>26</sup> of  $S(Q)$  in porous media can also be made.

### II. EXPERIMENT

#### A. Porous media samples

The MCM-41 was synthesized by the group of Patarin and Soulard at the Laboratoire de Matériaux Minéraux, UMR-CNRS, Mulhouse, France following the procedure of Corma *et al.*<sup>27</sup> It is the same MCM-41 batch as used and described previously by us.<sup>4,28</sup> The sample is a white powder of micrometer grain size. The silica grains contain parallel cylindrical pores ordered in a hexagonal lattice. N<sub>2</sub> isotherms were performed and analyzed by Mulhouse. Analysis of the isotherms using the standard Barrett, Joyner and Halenda (BJH) model<sup>29</sup> model yielded a mean pore diameter of 47 Å with a narrow pore diameter distribution of half width at half maximum (HWHM) of 1.5 Å. Analysis using the Brunauer, Emmett, and Teller (BET) model<sup>30</sup> model indicated a pore volume of  $v_p = 0.931$  cm<sup>3</sup>/gm. From diffraction measurements a lattice constant  $a = 63$  Å for the hexagonal lattice formed by the pores was found. Because of the presence of silanol and of incomplete polycondensation of the silica, the silica density was  $\rho = 1.8$  g/cm<sup>3</sup> rather than the usual 2.1 g/cm<sup>3</sup>. Thus the volume of the silica is  $v_{Sil} = 1/\rho = 0.55$  cm<sup>3</sup>/g giving a sample porosity of  $p = v_p/(v_p + v_{Sil}) = 63\%$ .

The MCM-41 sample investigated had a total mass  $M_S = 0.89$  g and occupied a volume  $V_S = 3.19$  cm<sup>3</sup>. The MCM-41 volume has three components,  $V_S = V_p + V_{Sil} + V_{IG}$ ; the volume of the pores, of the silica and of the intergranular space between the silica grains. When the sample cell is filled with helium, there is  $V_p = v_p M_S = 0.829$  cm<sup>3</sup> of confined helium in the pores,  $V_{Sil} = v_{Sil} M_S = 0.494$  cm<sup>3</sup> of silica and  $V_{IG} = V_S - (V_p + V_{Sil}) = 1.87$  cm<sup>3</sup> of bulk helium lying between the grains. Thus the volume of bulk helium between

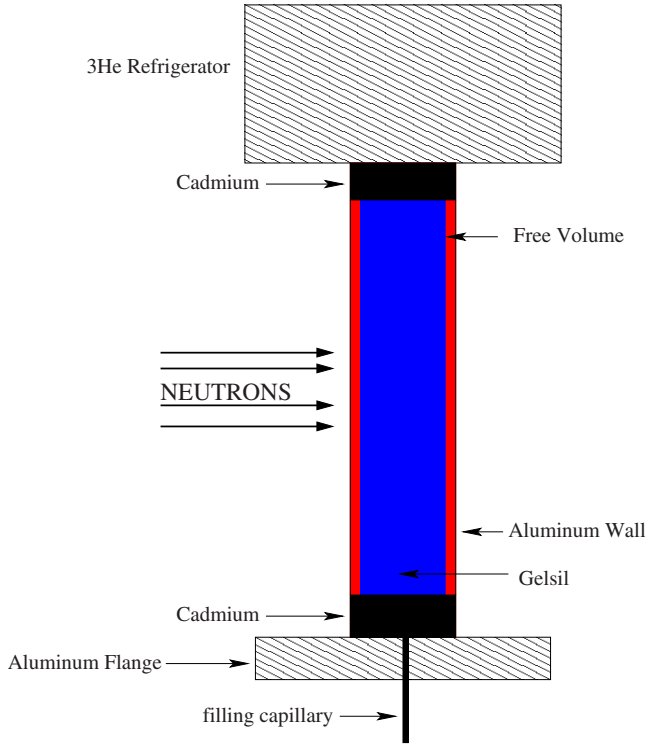


FIG. 1. (Color online) Schematic of the sample cell used for the MCM-41 and gelsil samples showing the gelsil sample. The gelsil has a pore volume of  $1.4 \text{ cm}^3$ . There is a volume  $0.6 \text{ cm}^3$  between the gelsil and the cell walls in the neutron beam and an additional volume  $0.3 \text{ cm}^3$  above and below the gelsil shielded from the neutron beam (reproduced from Ref. 4).

the grains is approximately twice the volume of helium confined in the  $47 \text{ \AA}$  diameter pores.

The  $34 \text{ \AA}$  gelsil was the same as used in Ref. 4 and is described in detail there. Gelsil has an aerogel-like pore structure, has a broad, Gaussian pore diameter distribution of HWHM of  $20 \text{ \AA}$  (see Fig. 1 of Ref. 4) and a pore volume of  $0.539 \text{ cm}^3/\text{gm}$  with a porosity of 58%. The sample consisted of two solid cylinders, one of diameter  $9.2 \text{ mm}$  and height  $18.3 \text{ mm}$ , the other of diameter  $9.0 \text{ mm}$  and height  $18.5 \text{ mm}$ , and had a total mass of  $2.58 \text{ g}$  and volume  $2.39 \text{ cm}^3$ . Both of the samples were flushed many times with helium gas at  $60 \text{ }^\circ\text{C}$  immediately prior to the neutron-scattering measurements.

### B. Neutron-scattering experiment

To conduct the neutron-diffraction measurements, the MCM-41 and  $34 \text{ \AA}$  gelsil samples were placed in a cylindrical aluminum sample cell of  $10.2 \text{ mm}$  internal diameter and  $40 \text{ mm}$  height. The cell used for the  $34 \text{ \AA}$  gelsil was the same as used in Ref. 4 for  $34 \text{ \AA}$  gelsil. A schematic of this cell is reproduced here as Fig. 1 for clarity. The gelsil cylinders were placed one on top of the other in the cell and there was a volume  $V=0.61 \text{ cm}^3$  between the gelsil and the cell walls. The helium in the neutron beam consists of  $1.39 \text{ cm}^3$  of confined helium in the gelsil pores and  $V=0.61 \text{ cm}^3$  of bulk helium around the gelsil sample. There was an addi-

tional volume of approximately  $0.3 \text{ cm}^3$  of bulk helium above the gelsil sample shielded from the neutron beam by a Cd ring (see Fig. 1).

In the MCM-41 case, the cell was the same except that the filling tube was at the top and the coldest point was at the bottom. With this geometry, the MCM-41 powder can fill the cell completely with no gaps between the powder and the cell walls without escaping via the filling tube under gravity. The helium in the neutron beam is thus the confined helium in the MCM-41 pores (volume  $V_p=0.829 \text{ cm}^3$ ) and bulk helium lying between the powder grains (volume  $V_{IG}=1.87 \text{ cm}^3$ ). Again, there was an additional volume of  $0.3 \text{ cm}^3$  of bulk helium lying above the MCM-41 sample shielded from the neutron beam by a Cd ring.

The sample and cell was cooled with a  $^3\text{He}$  cryostat which has a base temperature of  $0.4 \text{ K}$ . The cell was filled with helium at constant temperature and pressure on the bulk liquid/solid coexistence line with the filling capillary open. At the pressures above  $25.3 \text{ bars}$  considered here (e.g.,  $37.8 \text{ bars}$ ), the helium condenses as liquid in the porous media and as bulk solid helium in the open spaces. The pressure was determined from the temperature on the liquid/solid coexistence line and the known pressure-temperature relations on the line. When the cell is full, the capillary is blocked and the cell is isolated. The pressures quoted are the pressures on the bulk solid/liquid coexistence line when the cell becomes isolated. The neutron-scattering measurements were performed on the powder diffractometer D20 at the Institut Laue Langevin (ILL), Grenoble, France using an incident neutron wavelength of  $2.42 \text{ \AA}$ . The data were analyzed using the standard ILL data analysis package LAMP available on the ILL website.

## III. RESULTS

### A. MCM-41

To set the stage, we show the phase diagram of helium in MCM-41 determined from our measurements and that of bulk helium in Fig. 2. This diagram includes a horizontal dotted line at constant pressure  $p=37.8 \text{ bars}$  which extends from the bulk liquid/solid coexistence (melting) line ( $T=2.0 \text{ K}$  at  $p=37.8 \text{ bars}$ ) to  $T=0.4 \text{ K}$ . This line represents a cooling path of helium at constant pressure. We now describe the observed net  $S(Q)$  of the helium in the pores of MCM-41 (confined helium) plus the helium between the grains (bulk helium) as the sample cell is cooled along this line. This will clarify the origin of  $S(Q)$  and allow us to separate the  $S(Q)$  of the confined helium in the MCM-41 from that of the bulk helium between the grains. We begin on the bulk liquid/solid coexistence line at  $T=2.0 \text{ K}$  and pressure  $p=37.80 \text{ bars}$  with the cell open to a source of helium via a capillary. We track  $S(Q)$  as helium is added to the cell at constant  $T$  and  $p$ .

The ‘‘liquid’’ data in Fig. 3 is the net  $S(Q)$  of confined liquid in the MCM-41 and bulk liquid helium between the grains; i.e.,  $S(Q)$  of confined liquid plus bulk liquid. The sharp features at  $Q=3.1 \text{ \AA}^{-1}$  and  $Q=4.45 \text{ \AA}^{-1}$  in Fig. 3 arise from uncertainties in subtracting the scattering from the sample cell near the cell Bragg peaks to obtain the net  $S(Q)$ . The sharp features appear in all figures where a net  $S(Q)$  is

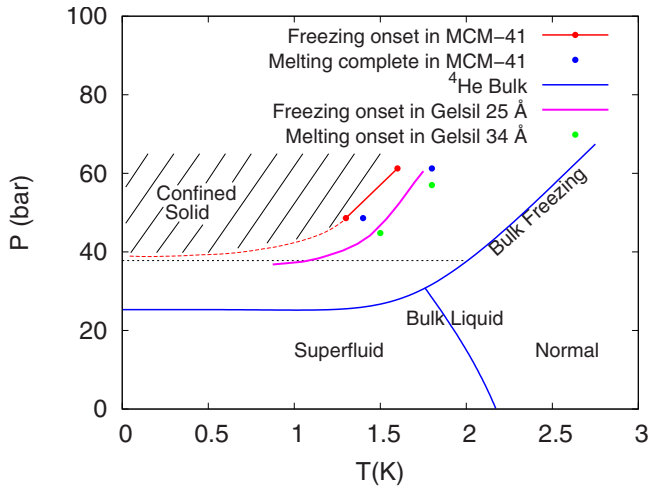


FIG. 2. (Color online) The phase diagram of helium confined in the present MCM-41, in the present 34 Å diameter gelsil and in 25 Å diameter gelsil (Ref. 31). The horizontal dotted line indicates the cooling of helium in MCM-41 at 37.8 bars discussed in Fig. 3. At 37.8 bars helium in MCM-41 remains liquid down to  $T = 0.4$  K. The dashed line (red) is an extrapolation of the freezing onset of helium in MCM-41 to low temperature.

shown. As more helium is added to the cell some of the bulk liquid between the grains solidifies. The “liquid+solid” data shows  $S(Q)$  when some of the bulk liquid has solidified. The helium is added slowly via the capillary in order to grow large crystals of bulk solid between the grains. The “solid”

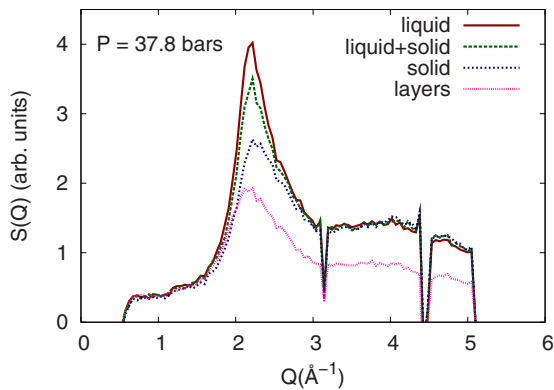


FIG. 3. (Color online) The net static structure factor  $S(Q)$  of liquid helium confined in MCM-41 and bulk helium between the grains of MCM-41. The temperature ( $T = 2.0$  K) and pressure ( $p = 37.8$  bars) are held constant on the bulk liquid/solid coexistence line and  $^4\text{He}$  is added to the cell. The  $S(Q)$  changes as the bulk helium around the MCM-41 solidifies when  $^4\text{He}$  is added at constant  $T$  and  $p$  via the open filling line. The liquid (red) data is  $S(Q)$  with bulk liquid around the MCM-41. The liquid+solid (green) data is  $S(Q)$  when some bulk liquid around the MCM-41 has solidified. The solid (blue) data is  $S(Q)$  when all the bulk liquid has solidified. The blue data represents  $S(Q)$  from liquid in the MCM-41, bound layers on the MCM-41 walls, and bulk solid around the MCM-41. The “layers” (magenta) data is  $S(Q)$  of the bound layers only which are clearly amorphous. The jagged features in  $S(Q)$  at  $Q = 3.1$  and  $4.45 \text{ \AA}^{-1}$  arise from background subtraction uncertainties around the Bragg peaks of the aluminum sample cell.

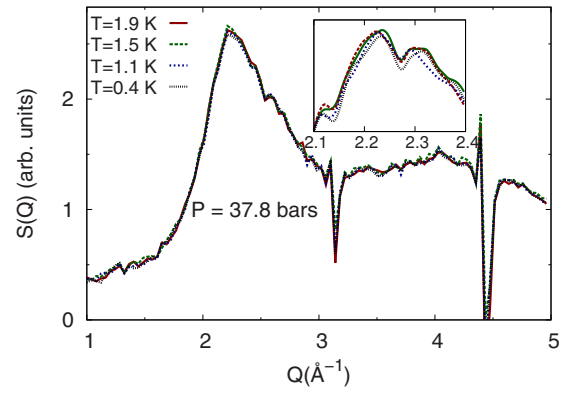


FIG. 4. (Color online) Net static structure factor  $S(Q)$  of liquid helium in MCM-41 at an initial pressure of 37.8 bars and temperature 2.0 K on the bulk liquid/solid coexistence line. The sample is cooled from 2.0 to 0.4 K. The  $S(Q)$  does not change indicating that the helium in the MCM-41 remains liquid down to 0.4 K.

data is  $S(Q)$  when sufficient helium has been added that all of the bulk helium between the grains has solidified. The difference between the solid and “liquid”  $S(Q)$  in Fig. 3 represents the intensity that has gone into the Bragg peaks. At the scattering angle shown in Fig. 3 none of the Bragg peaks of the bulk solid are observed. The aim of growing the bulk solid around the MCM-41 slowly at constant  $T$  and  $p$  is to obtain large enough crystals so that there are few bulk Bragg peaks and  $Q$  values can be found where the peaks are not observed. The crystalline size of the bulk helium solid is not known but the crystals are large enough that angles can be found readily where no Bragg peaks from the bulk solid are observed. The solid  $S(Q)$  in Fig. 3 arises from liquid within the MCM-41 and the layers of the helium tightly bound to the MCM-41 surfaces and possible diffuse scattering between Bragg peaks of the bulk solid between the grains. Finally, the magenta “layers” data is  $S(Q)$  arising from the helium layers that are tightly bound to the internal surfaces of the MCM-41. This data was taken with the cell at  $T = 5$  K with an atmosphere of helium gas in the cell so that the MCM-41 is empty except for the bound layers that remain on the walls. This data shows that the bound or “dead” layers on the MCM-41 walls are amorphous solid layers with an  $S(Q)$  that is similar to that of the liquid.

Figure 4 shows the net  $S(Q)$  from liquid helium in the MCM-41 and bound layers on the walls at  $p = 37.8$  bars. The cell is cooled in steps of 0.1 K from 1.9 to 0.4 K. No change in  $S(Q)$  on cooling is observed, except possibly a small reduction in the height of the main peak of  $S(Q)$ . The liquid in the MCM-41 remains liquid down to  $T = 0.4$  K so that  $p = 37.8$  bars is below the freezing pressure of liquid helium in the present MCM-41.

Figure 5 shows the net  $S(Q)$  as in Fig. 4 but at a higher pressure  $p = 48.6$  bars. At 48.6 bars there is a change in  $S(Q)$  on cooling in steps of temperature from  $T = 2.3$  to 0.4 K. The height of the main peak in  $S(Q)$  increases on cooling. The increase is somewhat larger on the low- $Q$  side of the main peak leading to the small lowering of the peak position (PP) in  $Q$ . Figure 6 shows  $S(Q)$  in the peak region on a larger scale as the cell is cooled in steps of 0.1 K. The increase in

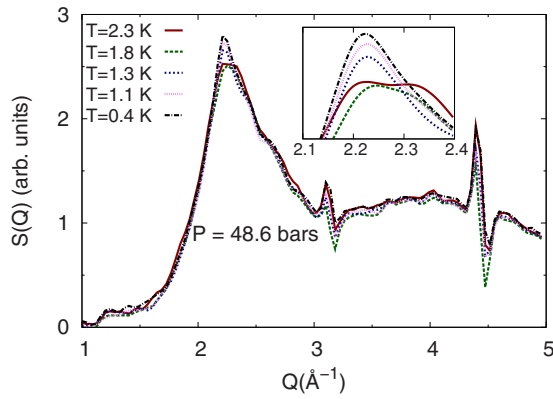


FIG. 5. (Color online) Net  $S(Q)$  of liquid helium in MCM-41 at an initial pressure of 48.6 bars and  $T=2.3$  K on the bulk liquid/solid coexistence line. The sample is cooled from 2.3 to 0.4 K. The  $S(Q)$  increases in the peak region of  $S(Q)$  on cooling. This increase is interpreted as solidification of the liquid to an amorphous solid. No Bragg peaks are observed. A similar change on solidification is observed on cooling from an initial pressure of 61.2 bars and  $T=2.5$  K.

peak height of  $S(Q)$  on cooling takes place between  $T=1.6$  K and  $T=1.3$  K, chiefly between 1.4 and 1.3 K. We interpret this change in  $S(Q)$  as solidification of the liquid to an amorphous solid at  $T=1.3$ –1.6 K at  $p=48.6$  bars. This interpretation is discussed in detail in the next section where a comparison with simulations of freezing in porous media is made. Figure 7 shows the change in  $S(Q)$  on increasing the temperature in steps of 0.1 K between  $T=0.4$  K and  $T=1.7$  K. On increasing the temperature, a decrease in the height of  $S(Q)$  back to the original value at  $T=1.7$  K takes place between 1.3 and 1.4 K. We interpret the decrease in the  $S(Q)$  as melting of the amorphous solid between  $T=1.3$  and 1.4 K. This change in  $S(Q)$  and its interpretation establishes a point on the melting curve of helium in MCM-41. It is interesting that once the change in  $S(Q)$  at melting/solidification has taken place there is little or no further change in  $S(Q)$  within each phase.

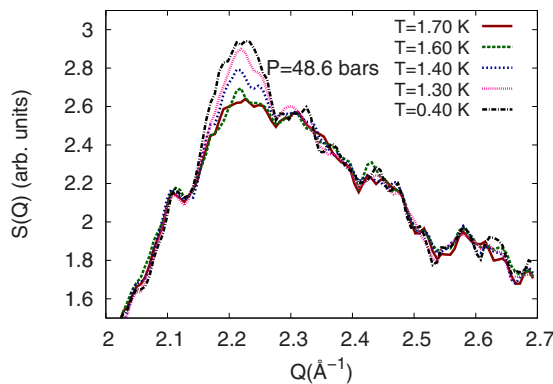


FIG. 6. (Color online) As Fig. 5 with a focus on the peak region of  $S(Q)$ . The change in  $S(Q)$  on cooling begins at  $T=1.6$  K and is largely complete at  $T=1.3$  K. This indicates an onset of solidification at  $T=1.6$  K (at 48.6 bars) with solidification complete at  $T=1.3$  K. At  $T=1.3$  K the pressure will be somewhat below 48.6 bars.

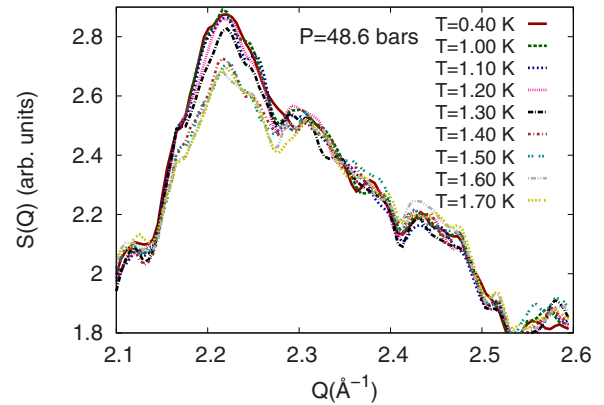


FIG. 7. (Color online) As Fig. 6 but the sample is heated from  $T=0.4$  to 2.3 K. The helium remains an amorphous solid up to 1.3 K. [ $S(Q)$  unchanged]. The onset of melting is at 1.3 K and melting appears to be complete by  $T=1.4$  K [ $S(Q)$  unchanged between 1.4 and 2.3 K].

Similar measurements of  $S(Q)$  were made at  $p=61.2$  bars. Beginning from the bulk liquid/solid coexistence line at  $T=2.5$  K, the liquid in the MCM-41 was cooled in steps of 0.1 K down to 0.4 K. As shown in the phase diagram in Fig. 2, the onset of freezing to an amorphous solid at  $p=61.2$  bars took place at  $T=1.6$  K. The solidification to an amorphous solid was associated with a small increase in the height of  $S(Q)$  in the peak region of  $S(Q)$  as at  $p=48.6$  bars. On increasing the temperature between 0.4 and 2.5 K, the onset of melting of the amorphous solid was at  $T=1.6$  K with melting complete at  $T=1.8$  K, as shown in Fig. 2.

In Fig. 8 we show the difference between  $S(Q)$  at  $T=0.4$  K and  $T=1.8$  K at 48.6 and 61.2 bars. The difference shows a peak at  $Q \approx 2.2$  Å<sup>-1</sup>. The positive and negative

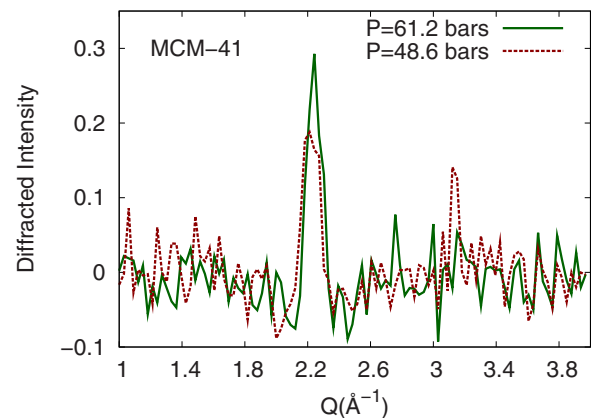


FIG. 8. (Color online) The difference between  $S(Q)$  of amorphous solid helium at 0.4 K and liquid helium at 1.8 K at  $p=48.6$  and 61.2 bars in MCM-41. The solid has additional intensity confined to a broad peak centered at  $Q \approx 2.2$  Å<sup>-1</sup> with FWHM  $\delta Q \approx 0.15$  Å<sup>-1</sup>. In the solid there is also a small decrease in intensity in the liquid like  $S(Q)$  around the broad peak. The difference in  $S(Q)$  indicates some partial ordering in the amorphous solid over distances of 5–10 Å. The small peak at  $Q=3.1$  Å<sup>-1</sup> arises from uncertainties in the background subtraction around a Bragg peak of the sample cell.

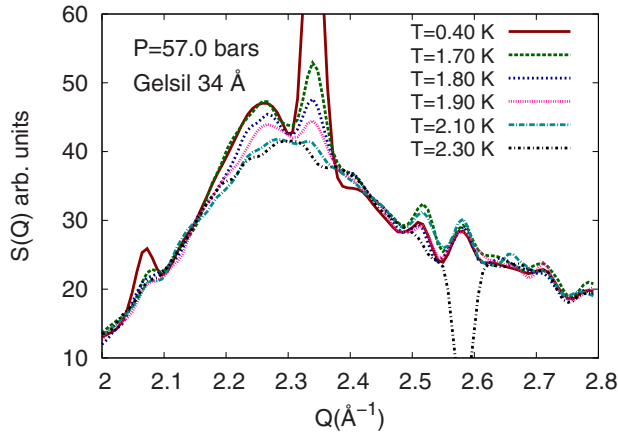


FIG. 9. (Color online) The change in  $S(Q)$  of helium at 57.0 bars in 34 Å gelsil on warming from  $T=0.4$  K to  $T=2.3$  K. There is a decrease in intensity of the broad peak of  $S(Q)$  centered at  $Q \approx 2.25$  Å<sup>-1</sup> on warming. The decrease begins at  $T=1.7$  K which is interpreted as the onset of melting of the amorphous solid. The sharp peak at  $Q=2.34$  Å<sup>-1</sup> is a Bragg peak of the bulk solid around the gelsil.

peaks  $Q=3.1$  and  $4.45$  Å<sup>-1</sup> arise from the uncertainties in the background subtractions near the Bragg peaks of the aluminum sample cell. Figure 8 shows that the difference between the amorphous solid and liquid  $S(Q)$  is confined to the main peak region of liquid  $S(Q)$  and is highly localized there. The main peak in the liquid  $S(Q)$  arises from short-range correlations in the atomic positions on the length of the interatom spacing. The increase in the peak height may arise from a tightening of these short-range correlations on freezing to an amorphous solid. The increase may also arise from some ordering on short length scales as discussed below. In the amorphous solid, there is also some loss of intensity in  $S(Q)$  around the peak shown in Fig. 8.

### B. Gelsil

Earlier, we determined  $S(Q)$  of helium as a function of pressure in 34 Å mean pore diameter gelsil.<sup>4</sup> At low pressure an  $S(Q)$  characteristic of bulk liquid helium is observed. As pressure is increased, the peak position of  $S(Q)$  moves to higher- $Q$  values as anticipated for a liquid under increasing pressure. At  $p \approx 35$  bars the liquid begins to freeze to an amorphous solid. Freezing is complete at  $p \approx 45$  bars. Freezing is indicated by a small increase in intensity in  $S(Q)$  at  $Q$  values just below the peak position of the liquid  $S(Q)$ , as observed here. No Bragg peaks were observed. Previously, we reported<sup>32</sup> an hcp solid Bragg peak from the solid in 44 Å gelsil but we now believe this Bragg peak arose from the bulk solid around the gelsil sample.

Figure 9 shows the  $S(Q)$  in the same 34 Å gelsil at  $p = 57$  bars as a function of decreasing temperature. At high temperature,  $T=2.3$  K, we observe an  $S(Q)$  characteristic of liquid in the gelsil (as in MCM-41). In Fig. 9 we also see Bragg peaks arising from the bulk solid around the gelsil sample. As temperature is decreased, the liquid in the gelsil freezes to an amorphous solid (e.g., at  $T=0.4$  K) with  $S(Q)$  increasing in the peak region as in MCM-41. For this

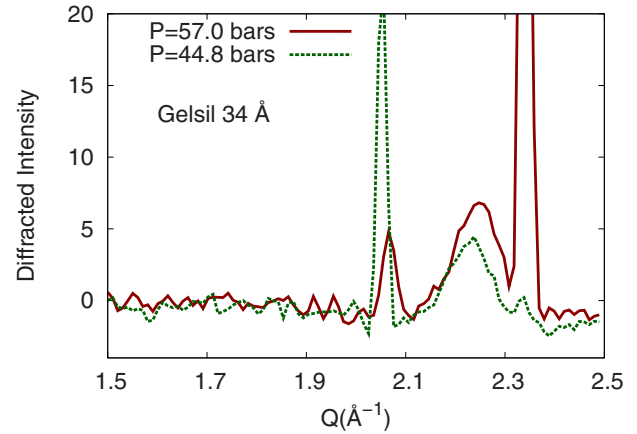


FIG. 10. (Color online) The difference between  $S(Q)$  of amorphous solid helium at 0.4 K and liquid helium at 1.8 K at  $p=44.8$  and 57.0 bars in 34 Å diameter gelsil. The solid has additional intensity confined to a single broad peak centered at  $Q \approx 2.25$  Å<sup>-1</sup> with FWHM  $\delta Q \approx 0.15$  Å<sup>-1</sup>. The sharp peaks at  $Q = 2.05$  and  $2.35$  Å<sup>-1</sup> are Bragg peaks from the bulk helium that is around the gelsil samples. The additional intensity in the solid phase indicates some partial ordering in the amorphous solid over length scales of order 5–10 Å.

sample, the data are not sufficiently precise to determine the freezing temperature. Since the Bragg peaks seen in Fig. 9 are observed at  $T=2.3$  K when there is clearly liquid in the gelsil, these peaks must arise from the bulk solid around the gelsil. Figure 10 shows the difference between  $S(Q)$  in the amorphous solid and the liquid at two pressures, the difference confined to a broad peak centered at  $Q=2.25$  Å<sup>-1</sup>. The intensity in the Bragg peaks in bulk solid helium can change with time and temperature as discussed, for example, in Refs. 4 and 33.

## IV. DISCUSSION

### A. Bound layers

The first layer of helium on silica glass surfaces is tightly bound to the surface. The second layer or part of the second layer is also tightly bound. These tightly bound layers are referred to as dead or “inert” layers. Some variation in the thickness of the dead layers is anticipated since the pore surfaces are rough and irregular. The tight binding of the dead layers to the surface is revealed in absorption isotherm measurements which show that the vapor pressure above these layers is very low.<sup>34</sup> Simulations of helium on a smooth glass surface<sup>26,35</sup> confirm that the first layer, but only the first layer, is tightly bound.

The dead layers do not contribute to superflow in liquid-helium films on porous media surfaces.<sup>36</sup> The superflow begins in the liquid or gas layers on top of the dead layers. Similarly the dead layers do not support phonon-roton (P-R) modes characteristic of superfluid helium.<sup>37</sup> In 25–44 Å mean pore diameter gelsils, for example, the P-R modes are observed only after the gelsil is 70% filled with helium at saturated vapor pressure (SVP).<sup>38,39</sup> At 70% filling there are one to two liquid layers on the top of the bound layers. Given

the rough nature of the surfaces, there will be variation in the thickness of these liquid layers as well as of the dead layers throughout the media. The dead layers also do not participate in the solidification of the inner liquid layers at higher pressures.<sup>26</sup>

The present measurements of  $S(Q)$  in Fig. 3 show unambiguously that the bound layers on MCM-41 walls at 5 K and SVP are amorphous solids. The shape of  $S(Q)$  is similar to that of bulk liquid helium. No Bragg peaks are observed. The position of the main peak in  $S(Q)$  is at  $Q=2.1\text{--}2.15 \text{ \AA}^{-1}$ , comparable to the peak position of liquid helium at  $p \approx 30$  bars suggesting a density  $n \approx 0.0265 \text{ \AA}^{-3}$ . An  $S(Q)$  characteristic of an amorphous solid is also observed for bound layers on gelsils<sup>4</sup> and on aerogel.<sup>40</sup> In all cases the peak position of the layer  $S(Q)$  is similar to that of the bulk liquid under modest pressure. This  $S(Q)$  may represent one or two layers or even more in crevasses.

In contrast, the first two bound layers on graphite surfaces form triangular lattice solids with lattice spacings of  $3.17 \text{ \AA}$  and  $3.54 \text{ \AA}$ , respectively. Lattices are observed on graphite probably because the surface is flat and the <sup>4</sup>He-carbon binding is somewhat greater. The spacing corresponds to first and second layer areal densities of  $n_A=0.115 \text{ \AA}^{-2}$  and  $n_A=0.092 \text{ \AA}^{-2}$ , respectively. Using the simple relation  $n=(n_A)^{2/3}$  (a cubic model) this translates to bulk densities of  $n=0.0390 \text{ \AA}^{-3}$  and  $n=0.0273 \text{ \AA}^{-3}$ , respectively. Layer densities are discussed further below.

### B. Confined helium

The central result of this paper is that liquid helium in  $47 \text{ \AA}$  diameter MCM-41 and  $34 \text{ \AA}$  diameter gelsil freezes to an amorphous rather than crystalline solid at pressures  $37.8 \leq p \leq 61.2$  bars. This is expected from simulations of classical liquids.<sup>24</sup> These show freezing to an amorphous solid if the pore diameter is  $d \leq 20\sigma$ , where  $\sigma$  is a hard core diameter of the atom ( $\sigma \approx 2.6 \text{ \AA}$  for helium). Thus we expect amorphous solid helium for  $d \leq 50 \text{ \AA}$ .

These simulations also find a number density,  $n$ , that is continuous across the freezing/melting transition, as observed here. The simulated density decreases with decreasing temperature in both phases but somewhat more rapidly in the liquid phase. The pair correlation function  $g(r)$  sharpens significantly with decreasing temperature but only in the amorphous phase below the transition temperature  $T_m$ . This sharpening arises from an increase in the number of angular correlations between nearest neighbors that are crystalline solidlike. In the liquid, 20% of the angular correlations are crystallinelike and this percentage increases gradually with decreasing temperature below  $T_m$  reaching 50% at  $(2/3)T_m$ . A sharpening of  $g(r)$  will lead to an increase in the height of the main peak of  $S(Q)$ , as we observe. However, the increase found in the classical simulations is gradual and takes place below  $T_m$  rather than the sudden increase just below  $T_m$  that we observe. The predicted increase arises from short-range correlations rather than long-range order.

As shown in Fig. 8, the difference between the amorphous solid and liquid  $S(Q)$  is a single peak localized at  $Q \approx 2.2 \text{ \AA}^{-1}$ . Quantum simulations<sup>26</sup> of helium in  $25 \text{ \AA}$  cylin-

dric pores under pressure show peaks in  $S(Q)$  at these  $Q$  values. In the quantum simulations the peaks arise from a long-range two-dimensional (2D) triangular lattice order developing within a given layer of helium with interatomic spacing  $R \approx 3 \text{ \AA}$ . At low pressures, comparable to those we have investigated, the intensity in the simulated peaks is small. The layering of the helium found in the simulations also represents an ordering, an ordering perpendicular to the walls. The spacing between the layers is  $R \approx 3 \text{ \AA}$  which would similarly lead to a peak in  $S(Q)$  at  $Q \approx 2\pi/R \approx 2 \text{ \AA}^{-1}$ . Thus the single peak in Fig. 8 could arise from this long-range ordering within a layer or perpendicular to the layers. The width of the peak in  $S(Q)$  (full width at half maximum,  $\text{FWHM} \approx 0.15 \text{ \AA}$ ) suggests ordering on length scales of  $5\text{--}10 \text{ \AA}$ . At significantly higher pressure, the simulation<sup>26</sup> finds a 2D crystalline solid phase in the layers (pressure-induced order). This is discussed further below.

The pressures quoted in Figs. 2–10 are the pressures on the bulk liquid/solid coexistence line at which the helium samples were grown as stated in Sec. II. On cooling below the bulk liquid/solid coexistence line to low temperature, between 2.0 and 0.4 K, for example, the pressure in the cell is expected to drop by 1.0–1.5 bars. This is the drop expected for bulk solid helium. Since the  $S(Q)$  from the helium in the pores changes little with temperature between 2.0 and 0.4 K, little or no volume change on solidification of the liquid to an amorphous solid in the pores is anticipated. Thus little or no additional pressure lowering arising from freezing in the pores is anticipated. But this is not well established. Similarly the small change in  $S(Q)$  on freezing indicates freezing in the pores is largely at constant volume. The size of the bulk helium crystals is large since we observed few Bragg peaks from these crystals. Also, at higher temperatures, above 1 K, there is continual change in the crystal structure of this bulk solid as signaled by movement of Bragg peaks, disappearance of Bragg peaks and appearance of new peaks as a function of time as observed by Burns *et al.*<sup>3</sup>

The PP of  $S(Q)$  provides an indication of the pressure. In bulk liquid helium at SVP and 14.9 bars (Ref. 41) the observed PP is at  $2.05 \text{ \AA}^{-1}$  and  $2.1\text{--}2.15 \text{ \AA}^{-1}$ , respectively. The peak position of  $S(Q)$  observed here at 37.8 and 48.6 bars is at approximately  $Q=2.2 \text{ \AA}^{-1}$  and  $2.25 \text{ \AA}^{-1}$ , respectively, with a PP at marginally higher  $Q$  at 61.2 bars (see Fig. 8). Calculations of  $S(Q)$  predict a PP at  $2.15\text{--}2.2 \text{ \AA}^{-1}$  at 25.3 bars and  $2.3 \text{ \AA}^{-1}$  at 150 bars. All these values appear to be reasonably consistent. Unfortunately the PP of  $S(Q)$  is difficult to determine precisely and it changes little with pressure at higher pressures<sup>42</sup> (e.g., the predicted PP at 300 bars is  $Q \approx 2.4 \text{ \AA}^{-1}$ ).

Wallacher *et al.*<sup>23</sup> have measured the  $S(Q)$  of helium confined in a  $70 \text{ \AA}$  mean pore diameter gelsil. The liquid helium in the  $70 \text{ \AA}$  pores and bulk solid helium around the gelsil were grown from bulk liquid at 70 bars until the filling capillary blocked. The confined liquid and bulk solid were then cooled. On cooling, the confined liquid in the gelsil pores solidified into a mixture of amorphous and crystalline solid. The crystalline component was identified as a bcc solid from the position of a broadened Bragg peak. Since we did not observe any Bragg peaks at all, we interpret our solid in  $34 \text{ \AA}$  gelsil pores as entirely amorphous. The appearance of

a crystalline component probably arises from the larger pore diameter gelsil investigated by Wallacher *et al.* Since the solid grows from the media walls inward and the first layer is amorphous, we expect a crossover from amorphous solid to crystalline solid after a certain number of layers of solid helium are grown. This is probably also the case in for helium in a bulk cell, depending on the wall material. Crossover to crystalline solid closer to the walls is expected at higher pressure.<sup>26</sup>

### C. Quantum simulations of confined helium

The variational Monte Carlo quantum simulations<sup>26</sup> noted above consider helium confined at  $T=0$  K in 25 Å diameter, smooth walled cylinders. The cylinders were fully filled with helium and the structure was investigated as a function of helium density. They find particularly that the helium orders in layers on the cylinder walls. The structure within a layer, whether liquidlike or solidlike, varies greatly from layer to layer. The atoms in the bound layer immediately adjacent to the pore walls (denoted the zeroth layer) are in a well of depth 160 K arising from interaction with the SiO<sub>2</sub> walls. In this zeroth layer, the atoms are dead in the sense that they are highly localized, form a defected triangular lattice structure and this structure does not change when structural changes take place in the inner layers. Boninsegni<sup>35</sup> also finds a single tightly bound dead layer on a smooth glass surface.

Essentially the “inert” layer does not participate in structural changes such as crystallization in the first and other layers within the pore when the pressure is increased. The areal density of the zeroth layer is predicted to be high,  $n_A \approx 0.12 \text{ \AA}^{-2}$ , which is somewhat higher than that observed for <sup>4</sup>He on graphite.<sup>43</sup> This translates<sup>26</sup> to a bulk density of  $n=0.046 \text{ \AA}^{-3}$  and a pressure of 780 bars. The translation from an areal density to a bulk density depends on the spacing between layers assumed and is not uniquely defined. A simple translation of  $n=(n_A)^{3/2}$  gives  $n=0.0416 \text{ \AA}^{-3}$ .

Our measurements of  $S(Q)$  show that the dead layer/layers on MCM-41 are amorphous rather than a defected triangularly lattice, probably because the MCM-41 walls are irregular. The PP of  $S(Q)$  also indicates a lower density,  $n=0.0265 \text{ \AA}^{-3}$  rather than  $n=0.042-0.046 \text{ \AA}^{-3}$  probably because the observed bound layer includes helium in the zeroth and in the first layers. These differences probably arise because the surfaces of MCM-41 and gelsils are irregular.

The simulated first layer is liquid at low pressure but solidifies to a triangular lattice at higher pressure. For example, at a density corresponding to bulk at  $n=0.024 \text{ \AA}^{-3}$  ( $p \approx 20$  bars) the first layer is liquid.<sup>26</sup> Solidification at higher pressure is characterized by the appearance of broadened peaks at  $Q \approx 2 \text{ \AA}^{-1}$  [just above the maximum of the liquid  $S(Q)$ ]. It is also accompanied by a significant loss of intensity in the liquid like  $S(Q)$  at other  $Q$  values. The new peak in  $S(Q)$  that we observe on lowering the temperature appears at the same  $Q$  value (see Fig. 6). However, the intensity in the peaks we observe is much smaller and there is little loss of intensity in  $S(Q)$  at other  $Q$  values. Thus the change in  $S(Q)$  we observe could signal some partial (long-range) ordering but the solid remains predominantly amorphous [i.e.,

little loss of intensity in the liquid like  $S(Q)$ ].

In the simulation, the second layer remains “liquid” up to higher densities (e.g.,  $n=0.0303 \text{ \AA}^{-3}$  and  $p \approx 100$  bars). At least, no sharp peaks in  $S(Q)$  are observed at this density. At high densities (e.g.,  $n=0.0348 \text{ \AA}^{-3}$  and  $p \approx 300$  bars), freezing to a crystalline phase is observed. These freezing pressures are much higher than the freezing pressures observed in small pore media (e.g., 40 bars). It is possible that solidification (to an amorphous solid) actually takes place at lower pressure in the simulations. In this interpretation, the appearance of Bragg peaks at higher pressure arises from crystallization of the amorphous solid at higher pressure. It would be interesting to test whether the amorphous solid we observe at lower pressures (i.e., up to 61.2 bars) actually develops a crystalline structure in response to increased pressure. Crystal formation of hard spheres under pressure is expected.

### D. Supersolid helium

Finally, the present results show that amorphous solid helium can be created in porous media and this may offer an opportunity to test the role of amorphous regions in supporting a superfluid density in solid helium. Unfortunately, torsional oscillator measurements<sup>44</sup> of the solid helium in 25 Å diameter gelsil, where the solid is amorphous,<sup>4</sup> find only a small  $\rho_S/\rho \approx 1\%$ . In this gelsil in the liquid phase some 70% of the liquid is in either the dead layers or in subsequent liquid layers that do not support superflow. Thus only a fraction (30%) of the sample is expected to contribute to superflow in the solid case. Similarly,  $\rho_S/\rho \approx 2.5\%$  in Vycor and  $\rho_S/\rho \approx 7\%$  in an unspecified porous media (Kim as quoted in Ref. 11) are reported. Tortuosity may play a role in reducing  $\rho_S/\rho$  in these media. It remains a challenge to find a media in which to test the possible role of amorphous solid helium in superflow.

## V. CONCLUSION

We have observed a transition in the static structure factor  $S(Q)$  of liquid helium in 47 Å pore diameter MCM-41 and 34 Å gelsil as the temperature is decreased. This transition is interpreted as solidification of the liquid to an amorphous solid. There is some order in the amorphous solid on length scales of 5–10 Å, as signaled by the appearance of a weak, broad peak in the solid which is absent in the liquid. The order is not hcp order and probably not bcc order. Rather, it is probably weak 2D order within layers of helium in the media, as found in quantum simulations.<sup>26</sup> It is not simply a transition to a glass for which no change in  $S(Q)$  is anticipated. The density does not change across the transition. The resulting phase diagram in the porous media is shown in Fig. 2.

It is interesting that helium in 47 Å diameter MCM-41 remains liquid at  $T=0.4$  K up to  $p=37.8$  bars, the pressure determined on the bulk melting line at  $T=2.0$  K. In previous measurements, we have observed a phonon-roton mode at  $T=0.07$  K in the liquid formed in this MCM-41 sample under exactly the same conditions, i.e., at  $T=2.0$  K and  $p=37.8$  bars on the bulk melting line.<sup>45</sup> At higher pressures a

phonon-roton mode is not observed.<sup>45</sup> These two results are consistent in identifying a liquid at  $T=0.4$  K up to  $p=37.8$  bars, the latter a liquid containing a Bose-Einstein condensate. It would be interesting to determine the onset of freezing more precisely near  $T=0$  K in porous media using  $S(Q)$ .

## ACKNOWLEDGMENTS

It is a pleasure to acknowledge the support of the Institut Laue Langevin and O. Losserand and A. Daramsy at ILL for valuable assistance with the experiments. This work was partially supported by U.S. DOE under Grant No. DOE-FG02-03ER46038.

- 
- <sup>1</sup>E. Kim and M. H. W. Chan, *Science* **305**, 1941 (2004).  
<sup>2</sup>E. Kim and M. H. W. Chan, *Nature (London)* **427**, 225 (2004).  
<sup>3</sup>C. A. Burns, N. Mulders, L. Lurio, M. H. W. Chan, A. Said, C. N. Kodituwakku, and P. M. Platzman, *Phys. Rev. B* **78**, 224305 (2008).  
<sup>4</sup>J. Bossy, J. V. Pearce, H. Schober, and H. R. Glyde, *Phys. Rev. B* **78**, 224507 (2008).  
<sup>5</sup>M. Boninsegni, N. V. Prokof'ev, and B. V. Svistunov, *Phys. Rev. E* **74**, 036701 (2006).  
<sup>6</sup>B. Hunt, E. Pratt, V. Gadagkar, M. Yamashita, A. V. Balatsky, and J. C. Davis, *Science* **324**, 632 (2009).  
<sup>7</sup>Ann Sophie C. Rittner and J. D. Reppy, *Phys. Rev. Lett.* **97**, 165301 (2006).  
<sup>8</sup>Ann Sophie C. Rittner and J. D. Reppy, *Phys. Rev. Lett.* **98**, 175302 (2007).  
<sup>9</sup>N. Prokof'ev, *Adv. Phys.* **56**, 381 (2007).  
<sup>10</sup>S. Balibar and F. Caupin, *J. Phys.: Condens. Matter* **20**, 173201 (2008).  
<sup>11</sup>J. T. West, O. Syshchenko, J. Beamish, and M. H. W. Chan, *Nat. Phys.* **5**, 598 (2009).  
<sup>12</sup>J. Day and J. R. Beamish, *Nature (London)* **450**, 853 (2007).  
<sup>13</sup>Y. Aoki, M. C. Keiderling, and H. Kojima, *Phys. Rev. Lett.* **100**, 215303 (2008).  
<sup>14</sup>Z. Nussinov, A. V. Balatsky, M. J. Graf, and S. A. Trugman, *Phys. Rev. B* **76**, 014530 (2007).  
<sup>15</sup>M. Boninsegni, N. Prokof'ev, and B. Svistunov, *Phys. Rev. Lett.* **96**, 070601 (2006).  
<sup>16</sup>D. M. Ceperley and B. Bernu, *Phys. Rev. Lett.* **93**, 155303 (2004).  
<sup>17</sup>B. K. Clark and D. M. Ceperley, *Phys. Rev. Lett.* **96**, 105302 (2006).  
<sup>18</sup>A. F. Andreev and I. M. Lifshitz, *Sov. Phys. JETP* **29**, 1107 (1969).  
<sup>19</sup>P. W. Anderson, *Science* **324**, 631 (2009).  
<sup>20</sup>M. Boninsegni, A. B. Kuklov, L. Pollet, N. V. Prokof'ev, B. V. Svistunov, and M. Troyer, *Phys. Rev. Lett.* **97**, 080401 (2006).  
<sup>21</sup>D. E. Galli, M. Rossi, and L. Reatto, *Phys. Rev. B* **71**, 140506(R) (2005).  
<sup>22</sup>D. E. Galli and L. Reatto, *J. Phys.: Condens. Matter* **12**, 6009 (2000).  
<sup>23</sup>D. Wallacher, M. Rheinstaedter, T. Hansen, and K. Knorr, *J. Low Temp. Phys.* **138**, 1013 (2005).  
<sup>24</sup>B. Coasne, S. K. Jain, and K. E. Gubbins, *Phys. Rev. Lett.* **97**, 105702 (2006).  
<sup>25</sup>M. Sliwinska-Bartkowiak, G. S. R. Dudziak, R. Gras, R. Radhakrishnan, and K. E. Gubbins, *J. Chem. Phys.* **114**, 950 (2001).  
<sup>26</sup>M. Rossi, D. E. Galli, and L. Reatto, *Phys. Rev. B* **72**, 064516 (2005).  
<sup>27</sup>A. Corma, Q. Kan, M. T. Navarro, J. Perez-Pariente, and F. Rey, *Chem. Mater.* **9**, 2123 (1997).  
<sup>28</sup>F. Albergamo, J. Bossy, P. Averbuch, H. Schober, and H. R. Glyde, *Phys. Rev. Lett.* **92**, 235301 (2004).  
<sup>29</sup>E. P. Barrett, L. G. Joyner, and P. P. Halenda, *J. Am. Chem. Soc.* **73**, 373 (1951).  
<sup>30</sup>S. Brunauer, P. H. Emmett, and E. Teller, *J. Am. Chem. Soc.* **60**, 309 (1938).  
<sup>31</sup>K. Yamamoto, Y. Shibayama, and K. Shirahama, *Phys. Rev. Lett.* **100**, 195301 (2008).  
<sup>32</sup>J. V. Pearce, J. Bossy, H. Schober, H. R. Glyde, D. R. Daughton, and N. Mulders, *Phys. Rev. Lett.* **93**, 145303 (2004).  
<sup>33</sup>N. Mulders, J. T. West, M. H. W. Chan, C. N. Kodituwakku, C. A. Burns, and L. B. Lurio, *Phys. Rev. Lett.* **101**, 165303 (2008).  
<sup>34</sup>F. Albergamo, J. Bossy, H. R. Glyde, and A. J. Dianoux, *Phys. Rev. B* **67**, 224506 (2003).  
<sup>35</sup>M. Boninsegni, *J. Low Temp. Phys.* **159**, 441 (2010).  
<sup>36</sup>J. D. Reppy, *J. Low Temp. Phys.* **87**, 205 (1992).  
<sup>37</sup>B. Fåk, O. Plantevin, H. R. Glyde, and N. Mulders, *Phys. Rev. Lett.* **85**, 3886 (2000).  
<sup>38</sup>F. Albergamo, J. Bossy, J. V. Pearce, H. Schober, and H. R. Glyde, *Phys. Rev. B* **76**, 064503 (2007).  
<sup>39</sup>O. Plantevin, H. R. Glyde, B. Fåk, J. Bossy, F. Albergamo, N. Mulders, and H. Schober, *Phys. Rev. B* **65**, 224505 (2002).  
<sup>40</sup>H. Godfrin, V. Lauter-Pasyuk, H. Lauter, and P. Leiderer, Institut Laue Langevin, Report No. 6-01-177, 1998 (unpublished).  
<sup>41</sup>D. G. Henshaw, *Phys. Rev.* **119**, 14 (1960).  
<sup>42</sup>L. Vranješ, J. Boronat, J. Casulleras, and C. Cazorla, *Phys. Rev. Lett.* **95**, 145302 (2005).  
<sup>43</sup>W. Thomlinson, J. A. Tarvin, and L. Passell, *Phys. Rev. Lett.* **44**, 266 (1980).  
<sup>44</sup>K. Shirahama (private communication).  
<sup>45</sup>J. Bossy, J. V. Pearce, H. Schober, and H. R. Glyde, *Phys. Rev. Lett.* **101**, 025301 (2008).